Single Nanostructure Electrochemical Devices for Studying Electronic Properties and Structural Changes in Lithiated Si Nanowires

*Matthew T. McDowell and Yi Cui**

Nanostructured Si is a promising anode material for the next generation of Li-ion batteries, but few studies have focused on the electrical properties of the Li-Si alloy phase, which are important for determining power capabilities and ensuring sufficient electrical conduction in the electrode structure. Here, we demonstrate an electrochemical device framework suitable for testing the electrical properties of single Si nanowires (NWs) at different lithiation states and correlating these properties with structural changes via transmission electron microscopy (TEM). We find that single Si NWs usually exhibit Ohmic *I–V* response in the lithiated state, with conductivities two to three orders of magnitude higher than in the delithiated state. After a number of sequential lithiation/delithiation cycles, the single NWs show similar conductivity after each lithiation step but show large variations in conductivity in the delithiated state. Finally, devices with groups of NWs in physical contact were fabricated, and structural changes in the NWs were observed after lithiation to investigate how the electrical resistance of NW junctions and the NWs themselves affect the lithiation behavior. The results suggest that electrical resistance of NW junctions can limit lithiation. Overall, this study shows the importance of investigating the electronic properties of individual components of a battery electrode (single nanostructures in this case) along with studying the nature of interactions within a collection of these component structures.

1. Introduction

In recent years, Si-based negative electrodes (anodes) for Li-ion batteries have been the focus of intense research efforts.[1–9] This is primarily because the theoretical specific capacity of Si is among the highest of known anode materials; it is about ten times that of commercial graphite anodes.[2] However, large volume changes and mechanical pulverization of particles during Li insertion/extraction have limited the capacity and cycle life of Si-based anodes.[7,10,11] Nanostructured Si anodes, especially one-dimensional nanostructures such as nanowires (NWs) and nanotubes (NTs), have shown resistance to fracture and have exhibited improved cycling performance.[2,3,6,12–15] Despite these advances, an understanding of the physical and electronic properties of lithiated Si has lagged behind battery performance studies. The structure of lithiated Si has been probed with a variety of techniques, including X-ray diffraction,[16,17] nuclear magnetic resonance,[5] and Raman spectroscopy.[18] In addition, other physical properties relevant to battery performance, such as mechanical properties and ionic and electronic conductivity, have also been examined.[18–21] Changes in electrical conductivity as Si is lithiated/delithiated are especially important for battery performance and have only received limited attention. Pollak *et al.* tested the conductivity of amorphous Si thin films during charging/discharging and found that lithiated Si was ~3.5 orders of magnitude more electrically conductive than delithiated Si.[18] This is significant because the electrical conductivity of Si plays a major role in determining the power and energy capabilities of the electrode; in general, high electrical resistance in a battery material can lead to incomplete reaction and to relatively high overpotentials that reduce the energy and power density of a battery.

In this study, we present a robust electrochemical device platform for probing the electronic transport properties and structural changes in single Si NW battery electrodes and NW ensembles at different stages of lithiation. In the field of nanoscience, single nanostructure electronic devices have been extremely useful for investigating electronic properties of nanomaterials,[22–25] which are not necessarily the same as those of the bulk or thin films. However, only a few researchers have utilized these devices to study the electronic properties of nanostructured battery materials.[26–28] Recent innovative research has been devoted to examining structural changes in nanostructured Li battery materials during electrochemical reaction via *in-situ* TEM, but this technique is primarily targeted at investigating structure and not electrical properties.[29] Our electrochemical device framework is designed to study electrical properties and structural changes in nanostructured battery materials. In addition, since studying battery nanostructures in situations mimicking actual devices is important to learn how

M. T. McDowell, Prof. Y. Cui
Department of Materials Science and Engineering
Stanford University
Stanford, CA, 94305, USA
E-mail: yicui@stanford.edu

DOI: 10.1002/aenm.201100258

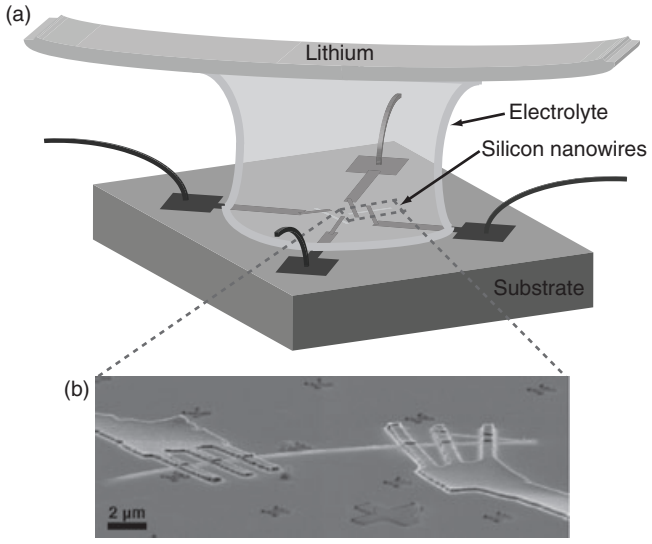

Figure 1. a) A schematic showing the architecture of a single NW electrochemical device. First, Si NWs are dispersed on a substrate and electrical contact is made through electron beam lithography and metal deposition. A drop of ionic liquid electrolyte is then placed over the NWs on the substrate, and a strip of Li metal is brought into contact with the electrolyte from above. In this way, single Si NWs can be lithiated/delithiated by controlling the voltage of the Si NW with respect to the Li metal counter/reference electrode. b) Side-view SEM image of a Si NW contacted by two arrayed Ti pads.

these nanostructures behave and interact with each other, our device allows for the investigation of the lithiation behavior of groups of nanostructures.

The experimental setup for the single NW electrochemical devices is shown in **Figure 1**a. This schematic shows a substrate on which Si NWs have been contacted with metal pads to allow for current-voltage measurements (the SEM image in Figure 1b shows a magnified view of a typical NW contacted with metal pads). A drop of ionic liquid electrolyte is placed on the substrate, and a strip of Li metal is brought into contact with the liquid from above without touching the substrate. In this way, a full electrochemical cell with a working electrode (the single Si NW), a counter/reference electrode (the strip of Li metal), and an electrolyte is formed, and the single Si NW can be reversibly lithiated/delithiated by controlling its potential with respect to the Li metal. Since this design incorporates a liquid electrolyte and a macroscopic (~2 mm by ~3 cm) Li metal counter electrode as the Li source, series resistance is minimized and lithiation/delithiation of the single Si NW readily occurs at the appropriate potentials. As a result, our single NW electrochemical device allows for more reliable electrochemical lithiation/delithiation than in previous devices that have incorporated microscopic thin-film counter electrodes and polymer electrolytes.[27] In addition, *ex-situ* transmission electron microscopy (TEM) can be used to observe structural changes since the devices are made on Si substrates etched to expose ~60 nm thick Si_xN windows suitable for electron beam transmission;[30] as such, this is a powerful method for relating structural changes and electronic properties in a specific individual NW.

Electrochemical lithiation/delithiation was carried out by sweeping the potential of the Si active electrode to a prescribed value vs Li/Li^+ from the open circuit voltage and then holding at that potential for 0.5–2 hours. Since the current due to the electrochemical reaction of a single Si NW is too small (~10 pA) to be monitored above the background current due to side reactions in this cell, holding the potential at a prescribed voltage ensures that lithiation/delithiation occurs without having to monitor the current. After the electrochemical treatment, the Li metal strip was removed and the electrolyte was washed away with acetonitrile, and then the *I–V* characteristics of the NWs were tested when the substrate was dry. For samples that were tested repeatedly with charge/discharge cycling or at different lithiation/delithiation potentials, the electrochemical treatment was repeated by adding another droplet of electrolyte and repositioning the Li metal strip over the substrate. All electrochemical procedures and *I–V* measurements were conducted inside an Ar-filled glove box.

2. Results and Discussion

2.1. Electrical Characterization

In order to determine the electrical characteristics of single NWs, we carried out two-terminal current-voltage measurements on NWs after the first lithiation and subsequent delithiation (**Figure 2**a). Figure 2c shows TEM images of a NW in a two-terminal device before (left) and after (right) lithiation at 70 mV, and the electron diffraction patterns (insets) show that the NW is completely amorphous after this electrochemical treatment. The linearity of the current trace in the lithiated state (black line in Figure 2a) indicates Ohmic behavior, and the conductivity of the lithiated NW (including contact resistance) is calculated to be 4 S cm^{-1} (see Supporting Information for details of the calculation). For lithiated NW devices that exhibited a linear *I–V* response, the conductivity after lithiating to 70 mV vs Li/Li^+ was usually measured to be between 1 and 10 S cm^{-1}; the average value was 3.6 S cm^{-1}. This conductivity is similar to that measured by Pollak *et al.* on lithiated amorphous Si thin films,[18] and it is higher than that for heavily N-doped amorphous Si (~10^{-1} S cm^{-1}).[31] Despite its very high lithium content, the measured conductivity of the Li-Si alloy is about four orders of magnitude less than that for metallic Li (~10^5 S cm^{-1});[32] this difference might be due to the amorphous nature of the Li-Si alloy. It was not possible to measure the conductivity of the Si NWs prior to lithiation because the doping level is too low, which results in low conductivity and high metal-NW Schottky junction resistance. However, a conductivity of 4 S cm^{-1} after lithiation represents an increase by several orders of magnitude over pristine NWs. The NW was delithiated by holding at 1.5 V vs Li/Li^+; the gray line in Figure 2a shows that the *I–V* curve is no longer linear in the delithiated state, and the current at 0.2 V decreases by a factor of about 500. The current response in the delithiated state for these devices was usually non-Ohmic, and the current was typically at least two to three orders of magnitude less than the current in the lithiated state. In many cases, the current in the delithiated

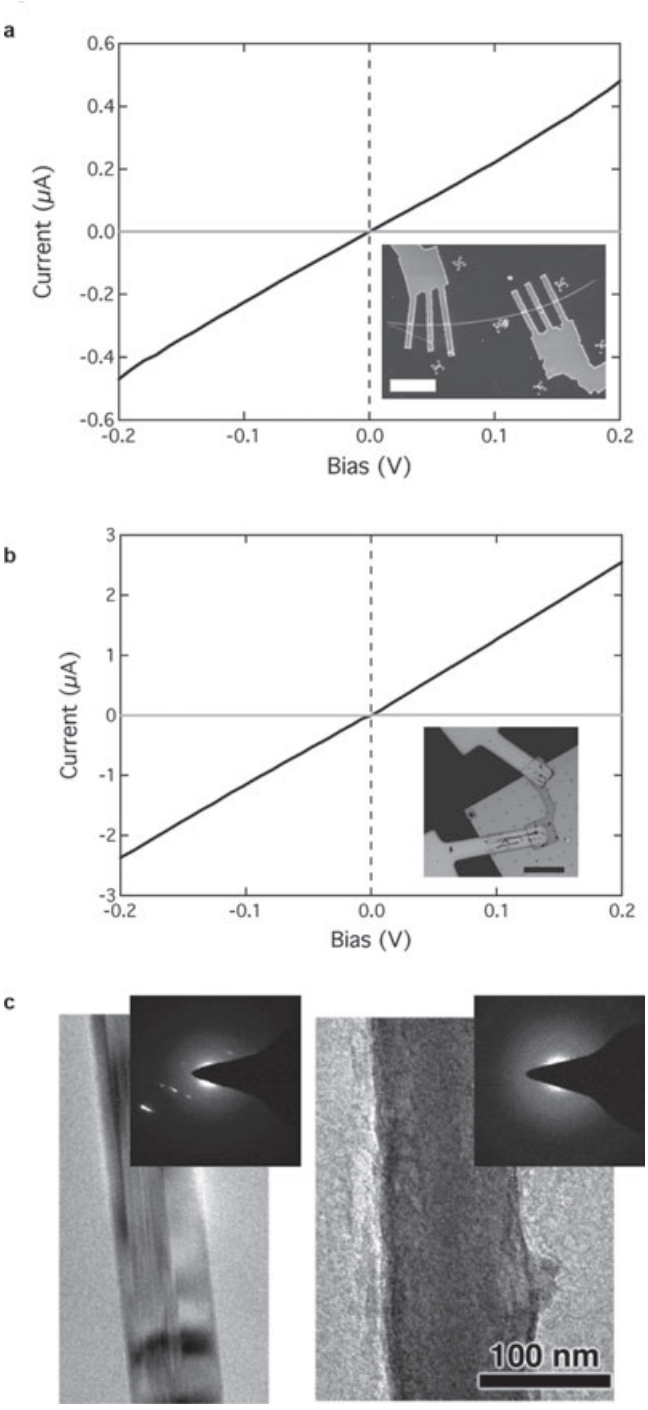

Figure 2. a) Current-voltage trace for a single NW in the lithiated (black) and delithiated (gray) states. The NW was lithiated by sweeping the potential from the open circuit voltage and holding at 70 mV vs Li/Li$^+$ for 80 min. The inset is a top-down SEM image of an example device (scale bar, 5 μm). b) Current-voltage trace for an amorphous Si thin film strip bridged between two electrical contacts in the lithiated (black) and delithiated (gray) states. The inset is a top-down optical image of the device (scale bar, 20 μm). c) TEM image of a single NW from a device before lithiation (left) and after lithiation (right) by sweeping to and holding at 70 mV vs Li/Li$^+$. The SAED patterns in the insets show that the initially crystalline Si NW becomes completely amorphous after lithiation at this potential.

state was convoluted with the background level of the test setup (a few pA).

In addition to current-voltage tests on NWs, we also measured the conductivity of patterned thin film strips of amorphous silicon. Figure 2b shows the current response of one of these samples in the lithiated (black) and delithiated (gray) states. The inset in Figure 2b shows an optical image of the sample; the film was 50 nm thick, 25 μm long, and 5 μm wide. Similarly to the NW sample, this device was lithiated by holding at 70 mV vs Li/Li$^+$. The device shows a linear *I–V* response, and the conductivity value calculated from the data in the lithiated state, 6 S cm^{-1}, is very similar to that from the NW device in Figure 2a. This suggests that the conductivity of the lithiated amorphous material does not depend on whether it starts as crystalline or amorphous. The delithiated current for this sample is about 500 times less than that in the lithiated state, which is similar to the previously mentioned Si NWs. To ensure that contact resistance does not significantly affect these data, we also performed four-terminal measurements on amorphous Si thin film strips. Due to their relatively large size, these films allowed for more reliable four-point measurements than on NWs. The average conductivity value from nine tested amorphous Si strip samples was 15.3 S cm^{-1}, which is only slightly higher than that measured from the NW and thin film two-terminal devices. This suggests that when the current-voltage characteristics are Ohmic, a two-terminal measurement gives a good estimate of the bulk conductivity. These results are shown in Table S1 in the supporting information.

In order to determine the effects of repeated cycling on the electrical characteristics of single NWs, we performed *I–V* measurements after each lithiation/delithiation step during electrochemical charge and discharge cycling. **Figure 3**a shows *I–V* curves from a single NW after each of four sequential lithiation steps (holding at 80 mV vs Li/Li$^+$), and Figure 3b shows *I–V* curves after the corresponding delithiation steps (holding at 1.0 V vs Li/Li$^+$). In the lithiated state (Figure 3a), the device exhibits linear *I–V* curves at low bias. Although there are some small variations in the *I–V* curves, they are mostly similar, with the calculated conductivity ranging between ~0.3 and 0.8 S/cm. In the delithiated state, the current is quite different after each cycle, as displayed in Figure 3b. After the first and second delithiation, the resistance of the device approaches the sensitivity limit of the experimental setup (~10^9–10^{10} Ω), so it is difficult to specify the actual resistance. After the third and fourth delithiation steps, the current is about an order of magnitude higher (0.2–1 nA at 0.2 V). Large variations in the delithiated *I–V* characteristics were common in these experiments, and they could be due to differences in the degree of delithiation of the single NW or changes in the nature of the contact resistance in the delithiated state. It is possible that residual Li atoms remain in the NW as dopants after delithiation, and slight variations in their concentration would result in differences in electronic conductivity.[31]

To probe how the electronic conductivity changes with lithiation voltage, two-terminal amorphous Si thin film devices like the one shown in the inset in Figure 2b were held at a series of sequentially lower lithiation potentials for at least 50 minutes each, and the *I–V* characteristics were measured after each lithiation step. Data from three different samples (squares, circles,

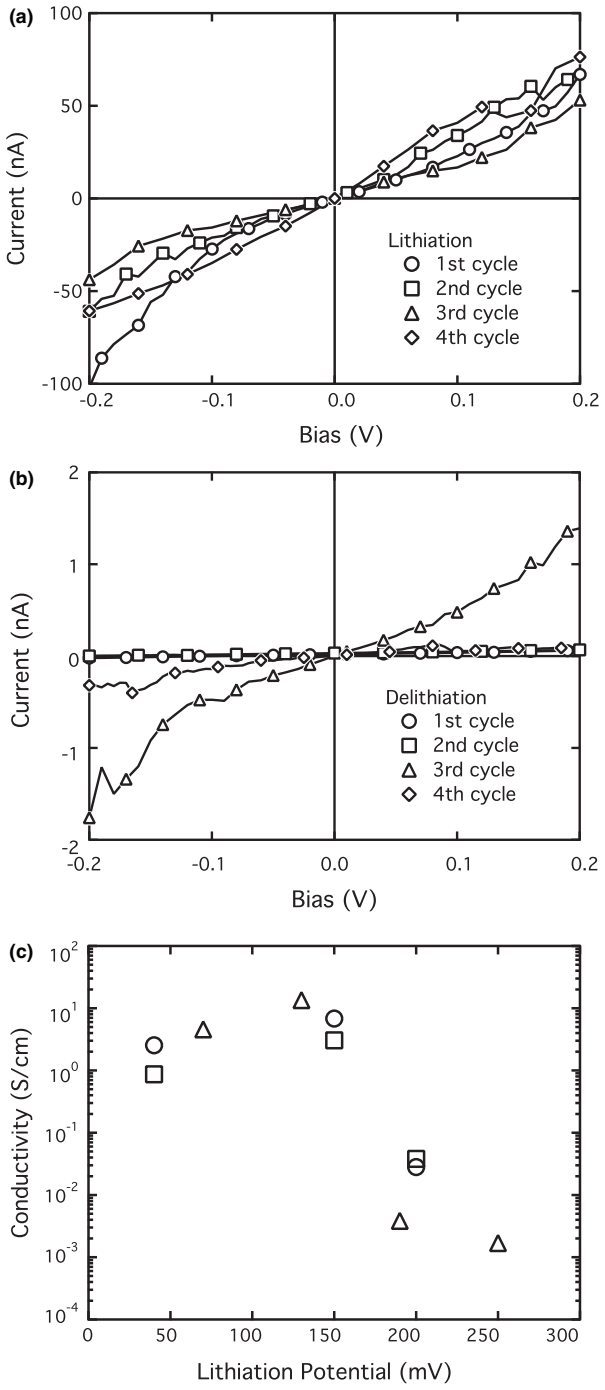

Figure 3. a) *I–V* characteristics of a single NW in the lithiated state after four successive charge/discharge cycles. The NW was lithiated by holding at 80 mV vs Li/Li^+. The current through the device is similar after each lithiation step. b) *I–V* characteristics of the same single NW in the delithiated state after four successive charge/discharge cycles. The NW was delithiated by holding at 1.0 V vs Li/Li^+. The current at 0.2 V after the first and second delithiation cycles is much lower than that after the third and fourth delithiation cycles. c) Conductivity from two-terminal measurements for three different amorphous Si thin film strip devices held at various potentials. Each sample was held at the specified lithiation potential for at least 50 minutes, and then the device was disassembled and the *I–V* characteristics were tested. These steps were then repeated for successively lower lithiation potentials. The three different symbols (square, circle, and triangle) represent the three different samples.

and triangles) are shown in Figure 3c. Based on cyclic voltammetry of much larger (~0.5 cm^2) amorphous Si thin film samples in conventional pouch-type electrochemical cells, formation of the Li-Si alloy phase occurs between ~350 and 0 mV (see Figure S1 in the supporting information).[18,33] Significant changes in electrical conductivity were measured below ~250 mV vs. Li/Li^+; the conductivity changes by about three orders of magnitude between 250 mV and 40 mV. These data are in close agreement with *in-situ* conductivity experiments conducted by Pollak *et al.*[18] Since the concentration of Li in Si generally increases as the potential is decreased, this substantial rise in conductivity below ~250 mV corresponds to the addition of more and more Li into the Li-Si alloy. The maximum conductivity value occurs between ~130 and 160 mV, with a slight decrease below ~100 mV. This decrease has been attributed to the formation of a less conductive alloy at low potentials.[18] These measurements show that compositional and structural changes during the initial stages of lithiation of amorphous Si are most important in determining the conductivity. As a note, crystalline Si is lithiated at lower potentials than amorphous Si (<~160 mV vs Li/Li^+), so the changes in conductivity in crystalline NWs would occur at different potentials compared to amorphous Si.[34]

2.2. TEM Characterization of NW Ensemble Devices

The aforementioned experiments have been aimed at probing the changes in electronic properties of single nanostructures. However, in a real battery electrode, both the properties of single nanostructures and the interactions among them determine the properties of the ensemble. Thus, it is also necessary to study the properties of collections of nanostructures. An important interaction between NWs in a battery electrode is electrical conduction across NW junctions. To probe this interaction, we studied the lithiation of a collection of Si NWs using *ex-situ* TEM in which individual NWs in the ensemble can be clearly resolved. Electrochemical devices were fabricated on TEM window substrates, and electrical connection was made to a single NW that was in physical contact with a group of other NWs. Lithiation was accomplished by sweeping the voltage of the contacting electrode from open circuit (~2.5 V) to 40 mV vs. Li/Li^+ and holding for 2.2 hours. TEM observation before and after the lithiation process reveals which NWs in the group amorphize due to lithiation.[34] Although amorphization does not necessarily signify full lithiation to the maximum alloy concentration, it does indicate that a NW has reacted with a significant amount of Li. Since the electrochemical lithiation reaction requires the transport of both electrons and Li^+ ions, this information is useful for deducing whether the reaction of a group of NWs is controlled by the transport properties of NWs themselves or by electronic resistance at junctions.

Figure 4 presents a low-magnification TEM image of an entire device (Figure 4a) and a series of magnified images of individual NWs (Figure 4b–i) after lithiation. The Ti pad for electrical connection contacts the primary NW at the bottom left of Figure 4a, and the primary NW is shown magnified along with a selected-area electron diffraction (SAED) pattern in Figure 4b. Figure 4c–i show magnified images of other NWs that are electrically connected to the primary NW through physical

contact; these NWs are variously within one and eight junctions removed from the primary NW. The white dotted line in Figure 4a traces an example electrical current path from the electrical contact at the primary NW to the NW that is furthest removed from the electrical contact. From Figure 4b, it is clear that the primary NW is completely amorphous, which indicates it has reacted with a substantial amount of Li. In addition, many of the secondary NWs are also fully amorphous, such as the NWs in the magnified TEM images in Figure 4c, d. Other secondary NWs, such as those in Figure 4e, f, g, and i, are partially lithiated with a crystalline Si core and an amorphous lithiated shell. A few NWs, such as that in Figure 2h, remain entirely crystalline. In all cases, completely amorphous NWs are connected back to the primary NW by other completely amorphous NWs. These details were consistent over all tested samples.

These observations give important insight into the nature of the interaction between NWs during lithiation. The main conclusion that can be drawn is that the electronic resistance at NW junctions is the primary factor that prevents more complete lithiation on this time scale. As shown by an example lithiated NW from a bulk electrode in the Supporting Information (Figure S2), lithiation of NWs by holding at potentials

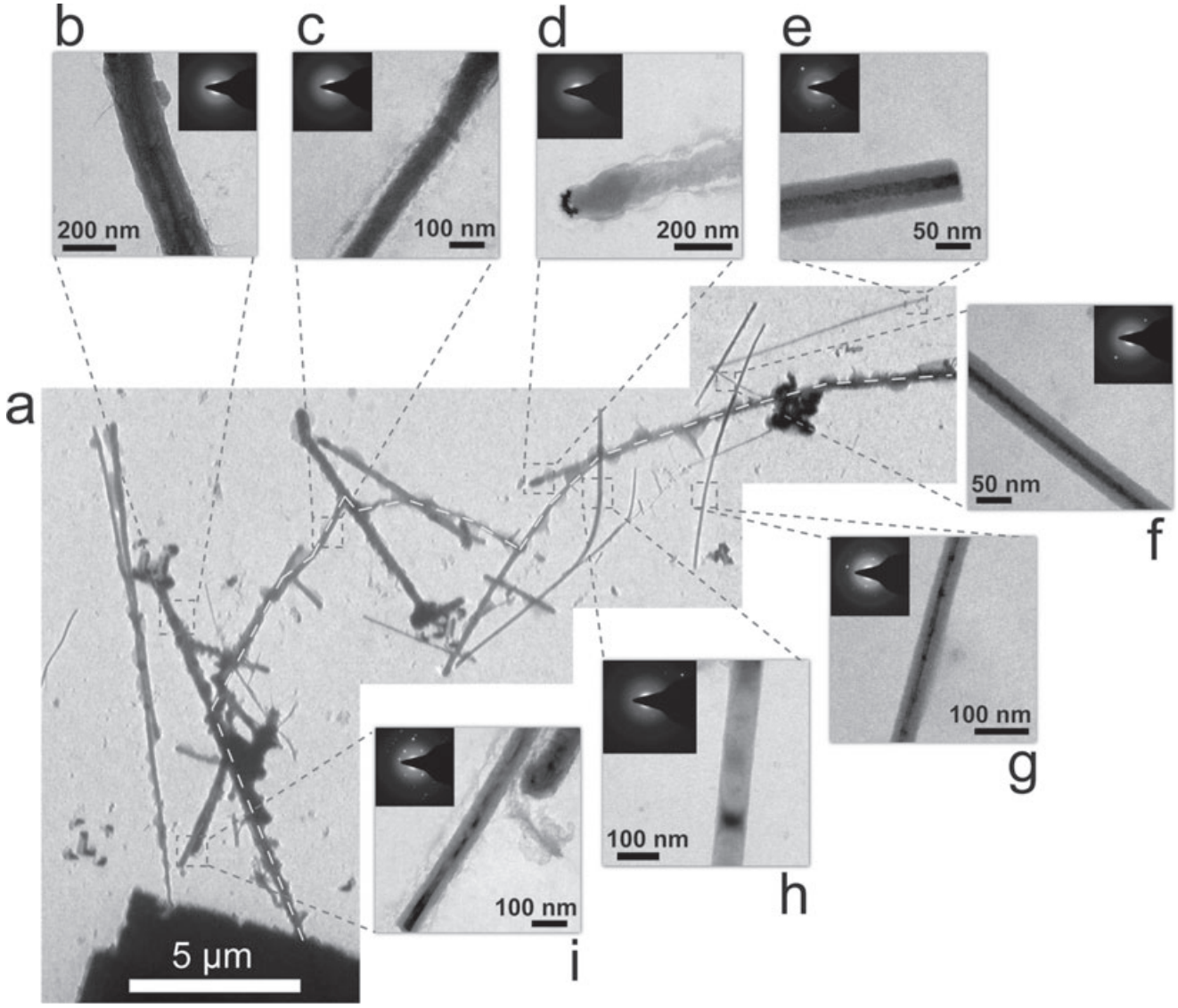

Figure 4. a) Low-magnification TEM image of a group of Si NWs in physical contact with each other. Electrical connection is made to the primary NW by the Ti pad at the bottom left of the device. The device has undergone electrochemical reaction by holding at 40 mV vs Li/Li^+, a potential at which crystalline Si is expected to fully amorphize due to reaction with Li. The white dotted line shows an example current path from the electrical contact through the NW array. b) Magnified TEM image and SAED pattern of the primary NW that is contacted by the Ti pad. This NW has been lithiated and is fully amorphous. c,d) Magnified TEM images of two more NWs that are also fully amorphous and are further separated from the primary NW by junctions between the NWs. e–i) Magnified TEM images of NWs that are partially lithiated and unlithiated. The partially lithiated NWs (e, f, g, and i) feature a crystalline Si core and an amorphous shell, while the unlithiated NW (h) is completely crystalline. These partially/fully crystalline NWs are dispersed throughout the device and the crystalline region is of constant thickness in each NW, which suggests that junction resistance between NWs is the limiting factor that prevents more complete lithiation.

ranging from ~110 mV to ~150 mV vs Li/Li^+ until equilibrium is approached results in a partially lithiated structure consisting of an amorphous shell surrounding a crystalline Si core. This partially lithiated structure results because these potentials are higher than necessary for full lithiation. Since partially crystalline core/shell NWs are observed in Figure 4 along with fully amorphous NWs, it seems that the partially lithiated NWs experience a different electrochemical potential than that of the applied voltage. The primary NW is held at 40 mV vs Li/Li^+, which is a potential at which full amorphization is expected to occur. However, the electrical resistance due to both the NWs themselves and junctions between NWs could dynamically alter the electrochemical potential of parts of the device during lithiation. After lithiation, most NWs are fully amorphous, which indicates that electronic and ionic transport in these NWs is sufficient for reaction on this time and length scale. However, partially and fully crystalline NWs are observed with 1) non-tapering crystalline core thickness and 2) varying degrees of separation from the primary NW. This suggests that the electrical resistance of the NWs themselves is not limiting on this time scale, but that the electrical resistance at NW junctions could alter the electrochemical potential of some of the NWs and therefore limit the reaction. If the electrical resistance of the NWs themselves was to limit the reaction on this time scale, one would expect to observe either tapering crystalline core thicknesses with thinner crystalline regions closer to the primary NW or incompletely lithiated NWs distributed only further from the primary NW. This is contradicted by the NW shown in Figure 4i, which is partially crystalline but directly contacts the primary NW, while other NWs further removed from the primary NW are completely amorphous. Since the degree of lithiation (thickness of the crystalline core) varies among different partially lithiated NWs, it seems that the junction resistance also varies from junction to junction, with presumably lower resistance and better electronic contact between NWs that are amorphous. Taken together, these observations indicate the importance of developing methods to ensure good electrical connections between nanostructures in real electrodes.

3. Conclusions

In conclusion, we have developed an electrochemical device framework that allows for the lithiation and delithiation of single nanostructures along with the ability to test *I–V* characteristics and characterize structural changes at different lithiation states. It was found that the electrical conductivity of individual Si NWs changes dramatically after the first lithiation and between lithiated/delithiated states. Measurements on Si thin films corroborated these data. In addition, *I–V* characteristics of single NWs were tested after a sequence of charge/discharge cycles; this demonstrates the robustness and stability of these devices. Finally, TEM was used to image NW junction devices, and it was concluded that junction resistance is an important factor that causes partial lithiation of some NWs. The electronic transport characteristics of lithiated Si directly impact many battery performance metrics, such as power density, so the understanding developed herein of the electronic properties of single lithiated Si NWs and how these NWs electrically interact in a configuration mimicking that of an actual battery electrode is critical. Since the electrical conductivity of Si is relatively low early in the lithiation process, it seems that electronic transport could play a role in limiting the kinetics of the lithiation reaction before significant alloying takes place, but that junction resistance could limit the extent of lithiation later in the lithiation process. To build on this work, it would be interesting to study the *I–V* characteristics of N- and P-doped single NWs as a function of Li content to determine whether doping modifies the transport behavior or junction resistance in any way. In addition, electrical tests to determine the junction resistance between lithiated Si NWs are important. Finally, the electrochemical devices described here could be used to correlate changes in electrical properties and structure in other nanostructured battery electrode materials.

4. Experimental Section

Device Fabrication: Silicon wafers with 60 nm Si_xN were used as substrates for all electrochemical devices. Electron beam lithography (EBL) or photolithography was used to pattern large electrical pads as shown in the schematic in Figure 1a, and 50 nm Ni (which is inert to Li reaction at low potentials) was thermally evaporated to form the pads. For the NW devices, NWs were grown via the vapor-liquid-solid mechanism on separate Si substrates using 50 or 100 nm Au nanoparticles (Ted Pella) as the catalyst.[35] The substrates were heated to 490 °C in a tube furnace, and then SiH_4 gas was flowed in at 50 sccm and 40 Torr for 12 minutes. For the TEM devices with groups of NWs, the NWs were grown on Si or steel substrates using a 30 nm evaporated Au film as the catalyst. After growth, the NWs were suspended in ethanol by sonication and spin-cast onto the device substrates. Using SEM (Philips XL30 SFEG), the positions of the NWs were determined with respect to the large Ni pads, and then EBL was used to write patterns for smaller Li-inert Ti pads to contact the NWs. The substrates were immersed in 2.5% HF for 30 sec to remove the oxide layer at the surface of the NW where it was to be contacted, 180–220 nm of Ti was e-beam evaporated onto the sample, and then the metal was lifted off to form the contact pads. For the amorphous Si thin film strip samples, EBL was used to pattern channels ~5–20 μm wide and 50–100 μm long that were directly on top of the large Ni pads at two or four locations. 50 or 60 nm thick amorphous Si was deposited by e-beam evaporation with subsequent lift-off to form the thin film strips.

At this point, each individual substrate sample was glued onto a glass slide, and external electrical connection was made by wirebonding the Ni pads to larger peripheral Au pads with Al wire bonds. The sample was then inserted into an Ar glove box kept below 3 ppm O_2 (MBraun). As described in the main text, a drop of ionic liquid electrolyte was placed on top of the NW device substrate, and then a strip of Li metal was bridged over the top of the substrate and gently pushed into contact with the electrolyte. The surface tension of the ionic liquid caused the drop to remain in contact with both the device substrate and the Li metal strip. The ionic liquid electrolyte employed was 1-ethyl-3-methylimidazolium bis(trifluoromethane-sulfonyl)imide (EMI-TFSI) with 0.8 M lithium bis(trifluoromethane-sulfonyl)imide (LiTFSI) salt. The ionic liquid electrolyte was employed to avoid the evaporation that would occur if traditional organic electrolytes were used.

Devices for TEM analysis were fabricated in the same manner, but Si substrates were used that had been etched from the back to form ~60 nm thick Si_xN windows on which the devices were made.[30] Briefly, double-side polished wafers were coated with ~60 nm low-stress Si_xN with low-pressure chemical vapor deposition. Using photolithography, the back of the wafer was patterned with squares, and the Si_xN was etching away

from these squares using plasma etching. With the patterned Si_xN on the back of the wafer as an etch mask, anisotropic KOH etching was then employed to etch through the wafer to create ~100 µm wide Si_xN-covered windows on the front of the wafer.

Electrochemical Reaction and Electrical Tests: Inside the glove box, electrical connection was made to the Li metal and to the wirebonded metal pads contacting the Si active material, and these leads were connected to a battery tester outside of the glove box via a coaxial cable adapter in the glove box wall. In this way, the Si active material was at the working electrode and the Li metal was the counter/reference electrode. Either a Biologic VMP30 or an Autolab PGSTAT100 was used for potentiostatic control of the electrochemical process. Electrochemical lithiation/delithiation was carried out by sweeping the potential of the Si active electrode to a prescribed voltage vs Li/Li^+ from the open circuit voltage at a sweep rate of 3 mV/s, and then holding at that voltage for 0.5–2 hours. The Li strip was then removed and the electrolyte was washed away with acetonitrile. The *I–V* characteristics were tested in the glove box when the sample was dry. An Agilent B1500A Semiconductor Device Analyzer was used for electrical tests. Two-terminal measurements were conducted by sweeping the voltage between two contact pads on a NW or thin film strip from –0.5 V to +0.5 V and monitoring the current. Four terminal measurements were conducted by driving an increasing current through two outside contact pads and monitoring the voltage between two inner contact pads.

For NW junction TEM devices, only one NW in the group of NWs was electrically contacted. After lithiation by sweeping to and holding at 40 mV vs Li/Li^+ for 2.2 hours, the substrates were washed and brought to a TEM (FEI Tecnai F20) in sealed glass vials. They were then placed in the sample holder and inserted into the TEM within ~20 sec to minimize air exposure.

Supporting Information

Supporting Information is available from the Wiley Online Library or from the author.

Acknowledgements

We thank S. Jeong for deposition of amorphous Si. We also appreciate the helpful comments on the manuscript from Z. Beiley and A. Jackson. A portion of this work was supported by the Assistant Secretary for Energy Efficiency and Renewable Energy, Office of Vehicle Technologies of the U.S. Department of Energy under Contract No. DE-AC02-05CH11231, Subcontract NO. 6951379 under the Batteries for Advanced Transportation Technologies (BATT) Program. A portion of this work was also supported by the Department of Energy, Office of Basic Energy Sciences, Division of Materials Sciences and Engineering, under contract DE-AC02-76SF0051, through the SLAC National Accelerator Laboratory LDRD project. Y.C. acknowledges support from the ONR Young Investigator Award and the King Abdullah University of Science and Technology (KAUST) Investigator Award (No. KUS-I1-001-12). M.T.M. acknowledges the National Defense Science and Engineering Graduate Fellowship, the National Science Foundation Graduate Fellowship, and the Chevron Stanford Graduate Fellowship for funding and support.

Received: May 17, 2011
Revised: June 17, 2011
Published online:

[1] A. Magasinski, P. Dixon, B. Hertzberg, A. Kvit, J. Ayala, G. Yushin, *Nat. Mater.* **2010**, *9*, 353.
[2] U. Kasavajjula, C. S. Wang, A. J. Appleby, *J. Power Sources* **2007**, *163*, 1003.
[3] C. K. Chan, H. L. Peng, G. Liu, K. McIlwrath, X. F. Zhang, R. A. Huggins, Y. Cui, *Nat. Nanotechnol.* **2008**, *3*, 31.
[4] V. L. Chevrier, J. R. Dahn, *J. Electrochem. Soc.* **2009**, *156*, A454.
[5] B. Key, R. Bhattacharyya, M. Morcrette, V. Seznec, J. M. Tarascon, C. P. Grey, *J. Am. Chem. Soc.* **2009**, *131*, 9239.
[6] T. Song, J. L. Xia, J. H. Lee, D. H. Lee, M. S. Kwon, J. M. Choi, J. Wu, S. K. Doo, H. Chang, W. Il Park, D. S. Zang, H. Kim, Y. G. Huang, K. C. Hwang, J. A. Rogers, U. Paik, *Nano Lett.* **2010**, *10*, 1710.
[7] J. R. Szczech, S. Jin, *Energy & Environmental Science* **2010**, *4*, 56.
[8] H. Kim, M. Seo, M. H. Park, J. Cho, *Angew. Chem., Int. Ed.* **2010**, *49*, 2146.
[9] A. Esmanski, G. A. Ozin, *Adv. Funct. Mater.* **2009**, *19*, 1999.
[10] R. A. Huggins, W. D. Nix, *Ionics* **2000**, *6*, 57.
[11] K. J. Zhao, M. Pharr, J. J. Vlassak, Z. G. Suo, *J. Appl. Phys.* **2011**, *109*, 016110.
[12] L. F. Cui, R. Ruffo, C. K. Chan, H. L. Peng, Y. Cui, *Nano Lett.* **2009**, *9*, 491.
[13] B. Hertzberg, A. Alexeev, G. Yushin, *J. Am. Chem. Soc.* **2010**, *132*, 8548.
[14] M. H. Park, M. G. Kim, J. Joo, K. Kim, J. Kim, S. Ahn, Y. Cui, J. Cho, *Nano Lett.* **2009**, *9*, 3844.
[15] R. Teki, M. K. Datta, R. Krishnan, T. C. Parker, T. M. Lu, P. N. Kumta, N. Koratkar, *Small* **2009**, *5*, 2236.
[16] T. D. Hatchard, J. R. Dahn, *J. Electrochem. Soc.* **2004**, *151*, A838.
[17] J. Li, J. R. Dahn, *J. Electrochem. Soc.* **2007**, *154*, A156.
[18] E. Pollak, G. Salitra, V. Baranchugov, D. Aurbach, *J. Phys. Chem. C* **2007**, *111*, 11437.
[19] V. A. Sethuraman, M. J. Chon, M. Shimshak, V. Srinivasan, P. R. Guduru, *J. Power Sources* **2010**, *195*, 5062.
[20] V. A. Sethuraman, V. Srinivasan, A. F. Bower, P. R. Guduru, *J. Electrochem. Soc.* **2010**, *157*, A1253.
[21] R. Ruffo, S. S. Hong, C. K. Chan, R. A. Huggins, Y. Cui, *J. Phys. Chem. C* **2009**, *113*, 11390.
[22] Y. Cui, C. M. Lieber, *Science* **2001**, *291*, 851.
[23] Y. Cui, X. F. Duan, J. T. Hu, C. M. Lieber, *J. Phys. Chem. B* **2000**, *104*, 5213.
[24] S. W. Chung, J. Y. Yu, J. R. Heath, *Appl. Phys. Lett.* **2000**, *76*, 2068.
[25] J. Y. Yu, S. W. Chung, J. R. Heath, *J. Phys. Chem. B* **2000**, *104*, 11864.
[26] Y. Yang, C. Xie, R. Ruffo, H. L. Peng, D. K. Kim, Y. Cui, *Nano Lett.* **2009**, *9*, 4109.
[27] L. Q. Mai, Y. J. Dong, L. Xu, C. H. Han, *Nano Lett.* **2010**, *10*, 4273.
[28] C. K. Chan, H. L. Peng, R. D. Twesten, K. Jarausch, X. F. Zhang, Y. Cui, *Nano Lett.* **2007**, *7*, 490.
[29] J. Y. Huang, L. Zhong, C. M. Wang, J. P. Sullivan, W. Xu, L. Q. Zhang, S. X. Mao, N. S. Hudak, X. H. Liu, A. Subramanian, H. Y. Fan, L. A. Qi, A. Kushima, J. Li, *Science* **2010**, *330*, 1515.
[30] D. T. Schoen, S. Meister, H. L. Peng, C. Chan, Y. Yang, Y. Cui, *J. Mater. Chem.* **2009**, *19*, 5879.
[31] W. E. Spear, P. G. Lecomber, *Solid State Commun.* **1975**, *17*, 1193.
[32] W. M. Haynes, Ed. *CRC Handbook of Chemistry and Physics*, CRC Press/Taylor and Francis, Boca Raton, FL **2010**.
[33] K. L. Lee, J. Y. Jung, S. W. Lee, H. S. Moon, J. W. Park, *J. Power Sources* **2004**, *129*, 270.
[34] C. K. Chan, R. Ruffo, S. S. Hong, R. A. Huggins, Y. Cui, *J. Power Sources* **2009**, *189*, 34.
[35] F. Patolsky, G. F. Zheng, C. M. Lieber, *Nat. Protoc.* **2006**, *1*, 1711.